AIChE

Simulation of Thermophysical Flow in Axisymmetric Nozzle with Expansion Chamber

Satoru Yamamoto, Ryo Matsuzawa, and Takashi Furusawa
Dept. of Computer and Mathematical Sciences, Tohoku University, Sendai 980-8579, Japan

DOI 10.1002/aic.12482
Published online December 28, 2010 in Wiley Online Library (wileyonlinelibrary.com).

Axisymmetric nozzle flows with a free-jet expansion are simulated considering several substances and several flow conditions, and the thermophysical properties in the nozzle and the free-jet region are predicted. The present numerical method is based on the preconditioning method developed by Yamamoto and the mathematical models of thermophysical properties of the substances. As numerical examples show, gas flows of carbon dioxide, water, and nitrogen under a subcritical pressure condition are first calculated. Calculated distances to the Mach disk are compared with the experimental results, and also the density distributions are compared among these three substances. Second, carbon dioxide flows while changing the pressure from subcritical to supercritical values are calculated and the effect of pressure on the flow field is investigated. Third, flows of water vapor with and without nonequilibrium condensation are calculated and the effect of condensation on the flow field is investigated. © 2010 American Institute of Chemical Engineers *AIChE J,* 57: 2629–2635, 2011
Keywords: numerical simulation, axisymmetric nozzle, free-jet expansion, supercritical fluids, nonequilibrium condensation

Introduction

A number of studies on the rapid expansion of supercritical solutions (RESS), which is a process for micronization of solids, has been reported.[1,2] In this process, first a supercritical solvent such as supercritical carbon dioxide with a dissolved solid is streamed in a capillary nozzle, and then the solution is expanded in an expansion chamber. Finally, rapid decreases of pressure and temperature nucleate nanoscale particles from the dissolved solid. In the past studies,[1,2] the nucleation and the growth of the particles were calculated using a simplified one-dimensional model. These studies indicated that the particles might have already been formed in the nozzle before the post-nozzle expansion. Therefore, understanding the thermophysical properties in the entire flow field is crucial for accurately predicting the micronization process. On the other hand, a rapid expansion of water vapor has been observed in the control valve of steam turbines: water vapor under high pressure and temperature conditions that leaked through the valve expanded rapidly and formed a supersonic flow with a free jet and a Mach disk. The rapid expansion also induced nonequilibrium condensation of the water vapor. Crist et al.[3] measured free-jet expansions using several substances while changing the pressure condition. Khalil and Miller[4] measured and calculated supercritical carbon dioxide flows with a free-jet expansion.

Our research group proposed a preconditioning method[5] for simulating both compressible flows and very slow flows such as natural convection. We calculated natural convection over a circular cylinder, and the results agreed well with those of the experiments. Our preconditioning method is fundamentally based on previous preconditioning approaches.[6,7] This method has also been applied to the simulation of natural convection over a circular cylinder in moist air considering condensation.[8]

In general, substances have their own thermophysical properties. These properties change according to the temperature and pressure conditions. Therefore, accurately predicting the thermophysical properties is absolutely necessary for obtaining the

Correspondence concerning this article should be addressed to S. Yamamoto at yamamoto@caero.mech.tohoku.ac.jp.

actual flow behavior. The preconditioning method[8] has been further coupled with the thermophysical properties of some substances programmed in a program package for thermophysical properties of fluids (PROPATH)[9] developed by Kyushu University. PROPATH has modeled most of the thermophysical properties for a primary set of 48 substances. For example, the equation of state (EOS) of carbon dioxide employed in PROPATH was standardized by the International Union of Pure and Applied Chemistry (IUPAC)[10] and the EOS for water was standardized by the International Association for the Properties of Water and Steam (IAPWS IF-97)[11] PROPATH can cover three states: gas, liquid, and supercritical fluid.

In this article, the preconditioning method[8] coupled with PROPATH is applied to calculate properties of flows through an axisymmetric nozzle followed by an expansion chamber, a system experimentally studied by Crist et al.[3] Predicting the thermophysical properties in the nozzle itself is crucial for understanding the RESS fabrication process.

As numerical examples, we first simulate gas flows of carbon dioxide, water, and nitrogen under subcritical pressure. Our calculated distances to the Mach disk are compared with the experiments by Crist et al.,[3] and the density distributions of these three substances are also compared with each other. Second, carbon dioxide flows while changing the pressure from a subcritical to a supercritical value are calculated and the effect of pressure on the flow field is investigated. Third, flows of water vapor with and without considering nonequilibrium condensation are calculated and the effect of the condensation on the flow field is investigated.

Numerical Methods

Fundamental equations

The fundamental equations, in this study, are based on the axisymmetric compressible Navier-Stokes equations and nonequilibrium condensation models. The set of fundamental equations is composed of the conservation laws of total density, momentum, total energy, density of liquid, and the number density of nuclei. In this study, we suppose that liquid droplets are sufficiently small; thus, we can assume a homogeneous flow without velocity slips among gas and liquid. The set of equations are written in vector form as

$$\frac{\partial \boldsymbol{q}}{\partial t}+\frac{\partial \boldsymbol{f}_l}{\partial x_i}+\frac{\partial \boldsymbol{f}_{vi}}{\partial x_i}+\boldsymbol{s}_1+\boldsymbol{s}_2=0, \tag{1}$$

where

$$\boldsymbol{q}=\begin{bmatrix}\rho\\ \rho u_1\\ \rho u_2\\ e\\ \rho\beta\\ \rho n\end{bmatrix},\ \boldsymbol{f}_i=\begin{bmatrix}\rho u_i\\ \rho u_1u_i+\delta_{i1}p\\ \rho u_2u_i+\delta_{i2}p\\ (e+p)u_i\\ \rho\beta u_i\\ \rho n u_i\end{bmatrix},$$

$$\boldsymbol{f}_{vi}=-\begin{bmatrix}0\\ \tau_{1i}\\ \tau_{2i}\\ \tau_{ki}u_k+\kappa\partial T/\partial x_i\\ 0\\ 0\end{bmatrix},$$

$$\boldsymbol{s}=\frac{u_2}{x_2}\begin{bmatrix}\rho\\ \rho u_1\\ \rho u_2\\ e+p\\ \rho\beta\\ \rho n\end{bmatrix},\ \boldsymbol{s}_2=-\begin{bmatrix}0\\ 0\\ (\rho_s-p)g\\ (\rho_s-p)gu_2\\ \boldsymbol{\Gamma}_c\\ I_c\end{bmatrix}.$$

The variables $\boldsymbol{q}$, $\boldsymbol{f}_i$, $\boldsymbol{f}_{vi}$, $\boldsymbol{s}_1$, and $\boldsymbol{s}_2$ are the vector of unknown variables, the inviscid flux, the viscous flux, the axisymmetric term, and the source term, respectively. Equation 1 can be further transformed to equations in general curvilinear coordinates. The set of equations are written by

$$Q_t+L(Q)=\frac{\partial Q}{\partial t}+\frac{\partial F_i}{\partial \xi_i}+\frac{\partial F_{vi}}{\partial \xi_i}+S=0, \tag{2}$$

where

$Q=J\boldsymbol{q}$, $F_i=J\left(\partial\xi_i/\partial x_j\right)\boldsymbol{f}_j$, $F_{vi}=J\left(\partial\xi_i/\partial x_j\right)\boldsymbol{f}_{vj}$, $S=J(\boldsymbol{s}_1+\boldsymbol{s}_2)$, and $J=\partial(x_1x_2)/\partial(\xi_1\xi_2)$.

The stress tensor τ_{ij} is given by

$$\tau_{lj}=\mu\left[\left(\frac{\partial u_i}{\partial x_j}+\frac{\partial u_j}{\partial x_i}\right)-\frac{2}{3}\delta_{ij}\frac{\partial u_k}{\partial x_k}\right], \tag{3}$$

and we assume that flows are laminar in this study.

The fundamental equations modified by the preconditioning method by Eq. 2 are written in general curvilinear coordinates as

$$\boldsymbol{\Gamma}\hat{Q}_t+L(\hat{Q})=\boldsymbol{\Gamma}\frac{\partial \hat{Q}}{\partial t}+\frac{\partial F_i}{\partial \xi_i}+\frac{\partial F_{vi}}{\partial \xi_i}+S=0, \tag{4}$$

where $\boldsymbol{\Gamma}$ is the preconditioning matrix and $\hat{Q}$ is the vector of unknown primitive variables defined by $\hat{Q}=\left[p\quad u_1\quad u_2\quad T\quad \beta\quad n\right]^T$. The elements in $\boldsymbol{\Gamma}$ are fundamentally the same as those in the formulation by Weiss and Smith[7]:

$$\boldsymbol{\Gamma}=\begin{bmatrix}\theta & 0 & 0 & \rho_T & 0 & 0\\ \theta u_1 & \rho & 0 & \rho_T u_1 & 0 & 0\\ \theta u_2 & 0 & \rho & \rho_T u_2 & 0 & 0\\ \theta h-(1-\rho h_p) & \rho u_1 & \rho u_2 & \rho_T h+\rho h_T & 0 & 0\\ \theta\beta & 0 & 0 & \rho_T\beta & \rho & 0\\ \theta n & 0 & 0 & \rho_T n & 0 & \rho\end{bmatrix}, \tag{5}$$

where $h=(e+p)/\rho$ and θ is the preconditioning parameter defined by

$$\theta=1/U_r^2-\rho_T(1-\rho h_p)/\rho h_T \tag{6}$$

with $\rho_T=\partial\rho/\partial T$, $h_T=\partial h/\partial T$, $h_p=\partial h/\partial p$, and U_r as the switching parameter. If U_r equals the physical speed of sound, then θ is zero and the fundamental equations are reduced to the compressible equations.

Equation 4 is solved by the finite-difference method based on a preconditioned flux-vector splitting scheme and a preconditioned lower upper symmetric Gauss-Seidel (LU-SGS) scheme.[8] Because the detailed expression has already been reported in a previous article,[8] we omit it here.

Thermophysical models

All of the thermophysical models in this study are taken from PROPATH[9] as external functions. The thermophysical

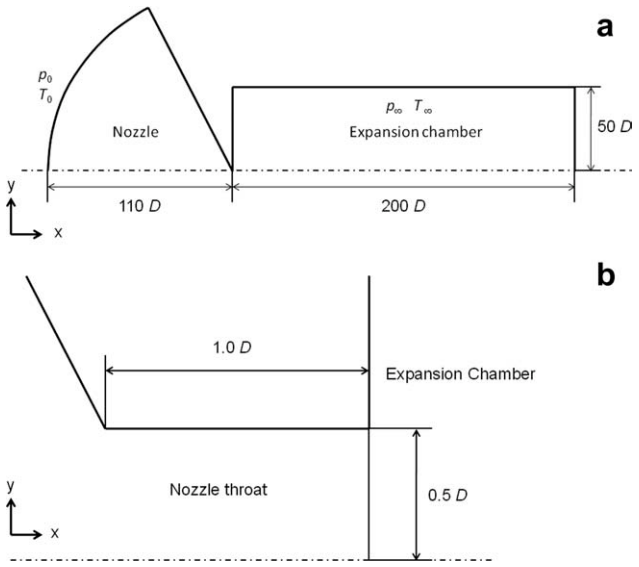

Figure 1. (a) Schematic of the axisymmetric nozzle and expansion chamber. (b) Schematic of the nozzle throat region.

properties for 48 substances under a wide range of pressure and temperature conditions are programmed in PROPATH. Most of the models of these thermophysical properties are approximated by polynomial equations derived from the existing theoretical equations or experimental data. PROPATH can cover all the states except for solid: gas, liquid, and supercritical fluid.

The model for carbon dioxide is explained here, because it is a typical model. The EOS model for carbon dioxide is defined by

$$p = \rho RT\left[1 + \omega \sum_{i=0}^{9} \sum_{j=0}^{J_i} a_{ij}(\tau - 1)^j(\omega - 1)^i\right], \tag{7}$$

where $\omega = \rho/\rho^*$, $\tau = T^*/T$, and the coefficients a_{ij} and the numbers J_i are defined in some other report.[10] The thermophysical properties such as isometric and isobaric specific heats can be derived from Eq. 7 as:

$$C_v = \int_0^\rho \frac{T}{\rho^2}\left(\frac{\partial^2 p}{\partial T^2}\right)_\rho d\rho + C_v^{\text{ideal}} \tag{8}$$

$$C_p = C_v + \frac{T\,(\partial p/\partial T)_\rho^2}{\rho^2\,(\partial p/\partial \rho)_T}, \tag{9}$$

respectively, where C_v^{ideal} is the isometric specific heat for the ideal gas. Because C_p is unique near the critical point, determining it accurately is very important for understanding the real physics underlying the phase interface. The molecular viscosity and thermal conductivity of carbon dioxide are also defined by polynomial equations. Thermophysical properties of other substances are approximated by polynomial equations. To save CPU time, we construct look-up tables from the PROPATH functions once and then interpolate the thermophysical properties from these tables.

Condensation model

Water vapor is occasionally condensed in fluid-machinery systems such as steam turbines. Condensation is basically governed by homogeneous nucleation and the nonequilibrium process. In this study, the condensation model developed by the authors[12] is applied to the present numerical method. Then, the mass generation rate Γ_c of water droplets in Eq. 1 is determined from the growth rate of water droplets approximated by Ishizaka et al.[13] as

$$\Gamma_c = \frac{4}{3}\pi\rho_\ell\left(I_c r_*^3 + 3\rho n r^2 \frac{dr}{dt}\right), \tag{10}$$

where ρ_ℓ is the density of liquid water. In this study, we employ the homogeneous nucleation rate I_c defined by Frenkel[14] and the growth rate of a water droplet dr/dt proposed by Schnerr and Dohrmann.[15]

Calculated Results

The present method is applied to flows in an axisymmetric nozzle with a free-jet expansion chamber experimentally studied by Crist et al.[3] In this article, the entire flow field from the nozzle region through the expansion chamber is calculated assuming an axisymmetric flow. Then, the thermophysical properties are occasionally changed from those under a supercritical condition to those under an atmospheric condition across the critical point through the nozzle. In addition, the flow is also accelerated from the static condition to a supersonic speed.

Figure 1a shows a schematic of the axisymmetric nozzle and the expansion chamber regions. The nozzle outlet connects both regions. The minimum diameter D of the nozzle throat is $D = 5 \times 10^{-5}$ m, and this nozzle is a capillary nozzle system. The length from the nozzle inlet to outlet on the x-axis is 110 times greater than the nozzle minimum diameter, where the nozzle outlet is located at $x = 0$. The expansion chamber has a length 200 times longer than D. Figure 1b shows a schematic of the nozzle throat. The length of the nozzle throat is the same as the nozzle diameter D.

Figure 2 shows a schematic of part of the computational grid. The grid has 101×41 grid points in the nozzle region and 201×121 grid points in the chamber region.

Figure 3 shows a schematic of a free jet formed in the expansion chamber. If the nozzle inlet is in a supercritical and static condition, then a supercritical flow accelerates through the nozzle and the supercritical-fluid phase changes to a gas phase in the nozzle. The flow ejected from the

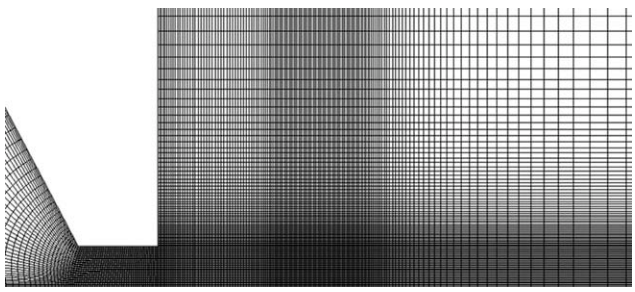

Figure 2. Schematic of part of the computational grid.

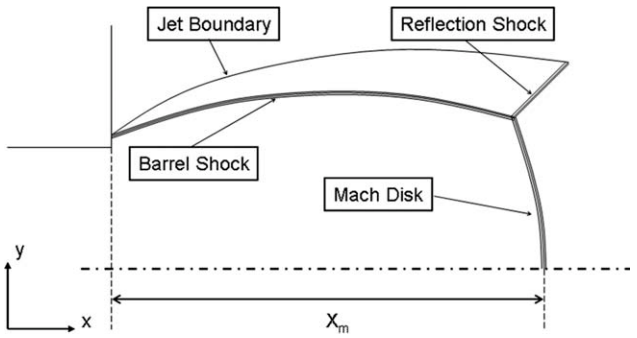

Figure 3. Schematic of a free jet with Mach disk and barrel shock.

nozzle outlet expands rapidly and produces a supersonic free jet. The jet typically forms two shock structures: barrel shocks and a Mach disk, as illustrated in Figure 3. At the solid walls of the nozzle region, adiabatic and no-slip boundary conditions are specified. At the chamber region's left boundary, adiabatic and no-slip conditions are specified; whereas, at its upper, lower, and outlet boundaries a free-stream boundary condition are specified.

Axisymmetric nozzle flows under subcritical conditions

We calculated the gas flows of carbon dioxide, water, and nitrogen that were experimentally studied by Crist et al.,[3] and compared the calculated distances to the Mach disk with the experiments. The nozzle outlet is assumed to be in an atmospheric condition and the outlet pressure p_∞ is set to 0.1013 MPa. The pressure ratio p_0/p_∞, where p_0 is the pressure at the nozzle inlet, is varied, as follows: for carbon dioxide, $p_0/p_\infty = 4.0$, 8.0, 10.0, 15.0, and 20.0; for water, $p_0/p_\infty = 4.0$, 10.0, 20.0, and 30.0; and for nitrogen, $p_0/p_\infty = 4.0$, 10.0, and 20.0. The inlet temperature T_0 and the outlet temperature T_∞ are specified as follows: for carbon dioxide, $T_0 = 400$ K and $T_\infty = 300$ K; for water, $T_0 = 600$ K and $T_\infty = 400$ K; and for nitrogen, $T_0 = 400$ K and $T_\infty = 300$ K. All cases are assumed to be under subcritical pressure and temperature conditions at the inlet.

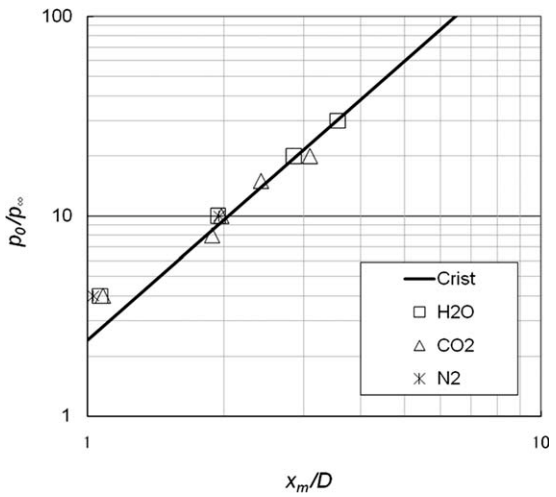

Figure 4. Calculated and experimental distances to the Mach disk.

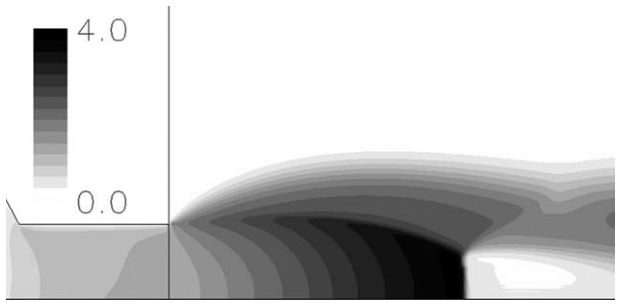

Figure 5. Calculated Mach number distributions.

Figure 4 plots our calculated values of the distance to the Mach disk X_m, and these values are compared with the experimental distances found by Crist et al.[3] Crist reported that the distance to the Mach disk depends only on the pressure ratio p_0/p_∞ and does not depend on the substance or the temperature. Except for the case of $p_0/p_\infty = 4.0$, all calculated values are near the line made by the experimental data. Figure 4 shows that the substance does not appear to affect the relationship between the distance and the pressure ratio.

Figure 5 shows the calculated Mach number distributions for the case of carbon dioxide with $p_0/p_\infty = 10.0$. The shock system including a Mach disk, a barrel shock, a reflection shock, and a jet boundary is clearly captured in Figure 5.

Figure 6 shows the distributions of the density ratio ρ/ρ_0 on the axis from the front of the nozzle throat to downstream of the Mach disk for all the three substances with $p_0/p_\infty = 10.0$. The distributions are almost identical, and the same distance to the Mach disk is obtained. However, slight discrepancies in the density ratio between the three substances are observed, especially in the nozzle region. These discrepancies may be due to differences in the thermophysical properties of the substances.

Axisymmetric nozzle flows of carbon dioxide under supercritical conditions

The previous cases assumed subcritical pressure and temperature conditions, without crossing the critical point. Next, we simulate carbon dioxide flows while varying the inlet and outlet pressure conditions, and the results calculated assuming a supercritical condition are compared with those of carbon dioxide gas. The inlet temperature is 350 K, the pressure ratio p_0/p_∞ is 10, and the outlet pressure p_∞ is varied at 0.1, 1.0, and 2.0 MPa that corresponds to CASE 1, CASE 2, and CASE 3, respectively. For CASE 1 we assume a totally gas condition; but for CASE 2 and CASE 3, we assume supercritical pressure and temperature conditions at the inlet, although these conditions are certainly changed to a gas condition through the nozzle throat.

Figure 7 shows the calculated distributions of the density ratio ρ/ρ_0 on the axis from the front of the nozzle throat to downstream of the Mach disk. Although all three cases have the same pressure ratio of $p_0/p_\infty = 10$, large discrepancies in the density ratio appear in the nozzle throat. Because the carbon dioxide in CASE 2 and CASE 3 is supercritical at the inlet and is changed to gas through the nozzle, the

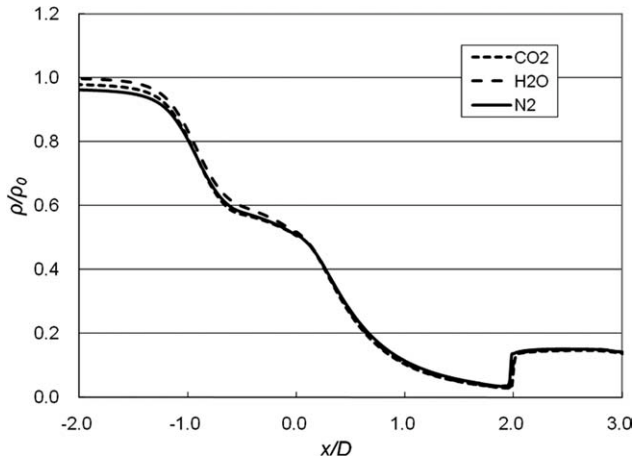

Figure 6. Calculated density distributions along the axis.

density in these cases changes more rapidly near the critical point than in CASE 1. In addition, the density gradient in CASE 2 is larger than that in CASE 3, probably because the pressure value at the inlet in CASE 2 is closer to the critical pressure value. This result suggests that the inlet pressure and temperature conditions certainly influence the nucleation process of nanoscale particles in the nozzle of RESS.

Axisymmetric nozzle flows of water vapor with nonequilibrium condensation

A rapid expansion of water vapor is observed in the control valve of steam turbines. Dry vapor that leaks through the valve rapidly expands to form a supersonic flow with a free jet and a Mach disk. The rapid expansion also induces nonequilibrium condensation of water vapor. The flow system is quite similar to the RESS process. In this article, the axisymmetric nozzle shown in Figure 1 is further applied to flows of water vapor. In the present system, we assume that dry vapor at the inlet under subcritical pressure and temperature conditions streams in the nozzle. Then, the vapor expands to a supersonic flow at the expansion chamber, and homogeneous nucleation and nonequilibrium condensation occur in the supersonic region. As the inlet boundary conditions, the inlet temperature and pressure are $T_0 = 600$ K and $P_0 = 20.26$ MPa, and the outlet pressure is $p_\infty = 0.1013$ MPa; hence, $p_0/p_\infty = 20$.

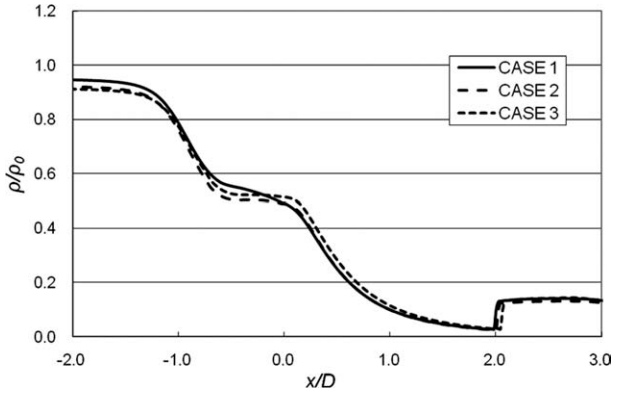

Figure 7. Calculated density distributions along the axis.

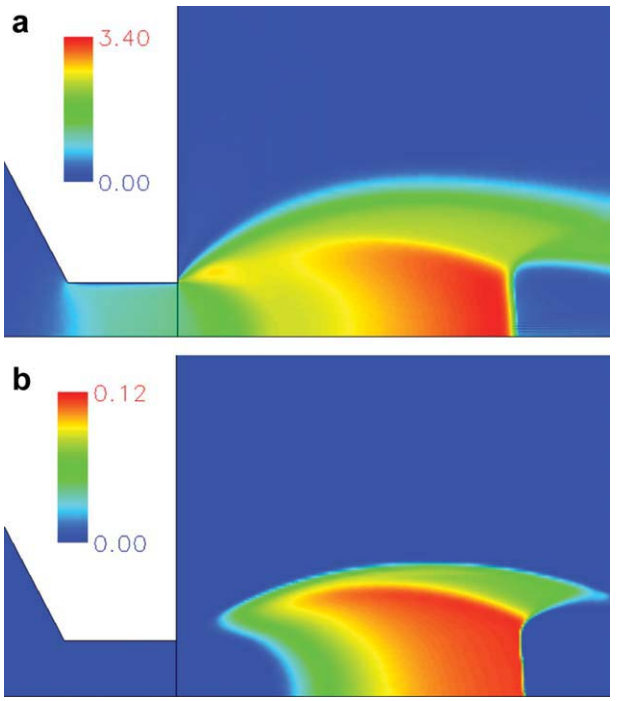

Figure 8. Calculated Mach numbers and condensate mass fractions.

(a) Mach number distributions. (b) Condensate mass fractions. [Color figure can be viewed in the online issue, which is available at www.wileyonlinelibrary.com.]

Figures 8a,b show the calculated Mach number distributions and the condensate mass fractions. The Mach number changes through the nozzle throat, and it reaches more than 3.0 at the expansion chamber. Figure 8a clearly shows a Mach disk and a barrel shock, whereas Figure 8b shows a condensed supersonic region. The condensate mass fraction increases gradually toward the Mach disk and the barrel shock, and its value decreases rapidly after the shocks because of the evaporation of water liquid in the subsonic region. The Mach number distributions can be compared with those of the CO_2 case without condensation in Figure 5. Although the quantitative comparison is difficult because of the different substance and flow conditions, the Mach number distributions in Figure 8a are certainly influenced by the condensation. The length of the Mach disk is longer and the jet boundary spreads more widely than those in Figure 5.

Next, the density and Mach number obtained considering condensation are compared with those obtained ignoring condensation. Figures 9a–c show the calculated density distributions, the Mach number distributions, and the temperature distributions, respectively, through the nozzle and the expansion chamber along the axis. The density distributions are almost identical to each other except at the location of the Mach disk. The distributions can be also compared with those in Figure 6. Although the flow conditions are different and the values are normalized in Figure 6, the density behavior in the nozzle is quite similar to that using water in Figure 6 because of the same substance in same subcritical

conditions. The Mach disk is shifted downward for the case where condensation occurs. The reason may be explained by the Mach number distributions in Figure 9b and the temperature distributions in Figure 9c. The Mach number relatively decreases after the point where the onset of condensation occurs due to the release of latent heat as shown in Figure 9c when water vapor liquefies. The decrease of the Mach number may delay the formation of the Mach disk.

Finally, we further clarify the effect of condensation on the dislocation of the Mach disk with additional calculations where we use the following pressure ratio values: $p_0/p_\infty =$ 4, 10, 15, and 30. Figure 10 plots our calculated values of the distances to the Mach disk while changing p_0/p_∞ with and without considering condensation and these values are compared with the experimental distances found by Crist et al.[3] Except for $p_0/p_\infty = 4$, the distances to Mach disk are increased by condensation.

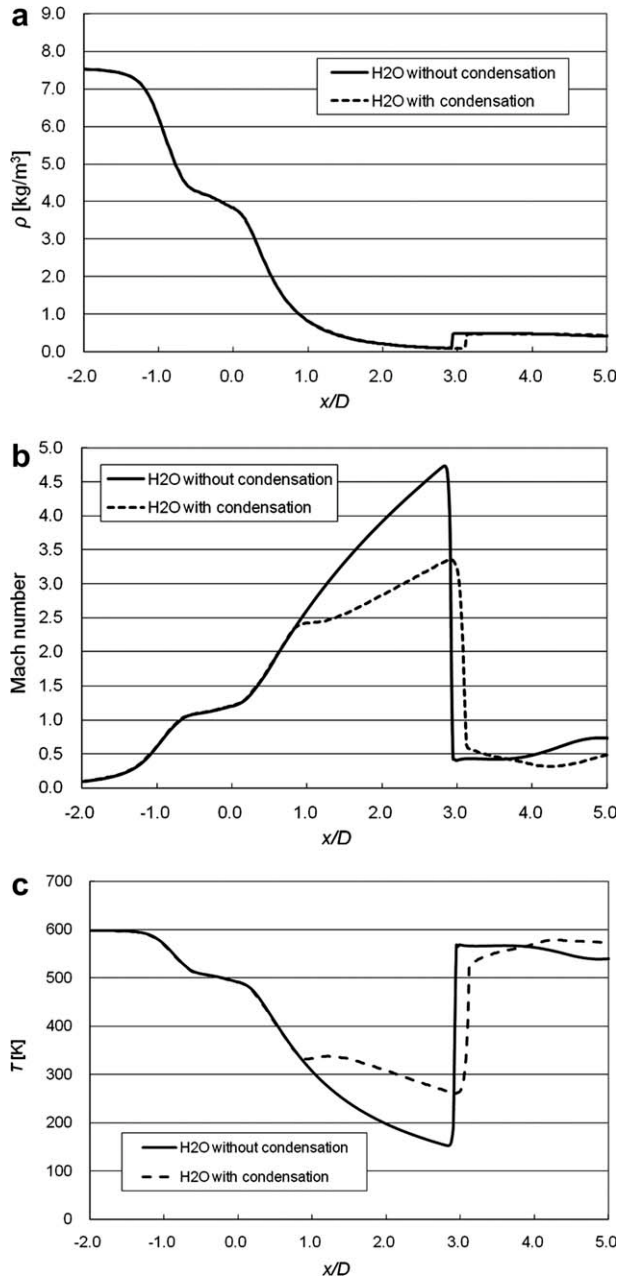

Figure 9. Comparison of calculated results with and without condensation.

(a) Calculated density distributions along the axis. (b) Calculated Mach number distributions along the axis. (c) Calculated temperature distributions along the axis.

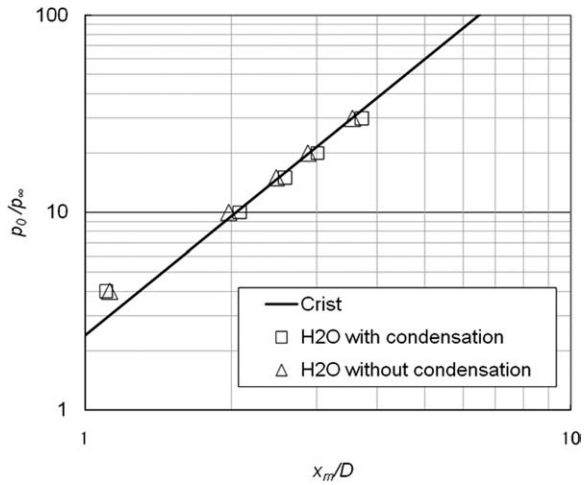

Figure 10. Calculated distance to the Mach disk compared with experiments.

Concluding Remarks

Axisymmetric nozzle flows with a free-jet expansion were numerical investigated by our preconditioning method coupled with PROPATH. Distances to the Mach disk for the flows of carbon dioxide, water, and nitrogen under a subcritical pressure condition were calculated, and our calculated values were in good agreement with the experiments by Crist. Next, properties of carbon dioxide flows while changing the pressure at the inlet from a subcritical value to a supercritical one were calculated. Then the calculated density distributions for the supercritical pressure condition were quite different from those for the subcritical pressure condition, especially in the nozzle throat. This result suggests that accurate evaluation of the thermophysical properties in the nozzle is quite valuable for accurately predicting the nucleation process of nanoscale particles in the RESS process. Finally, properties of the flows of water vapor considering nonequilibrium condensation were calculated and the calculated distances to the Mach disk were compared with those from the experiments by Crist. We found that condensation increased the shock distances compared to the results without condensation.

Notation

C_p = specific heat at constant pressure
e = total internal energy per unit volume
g = gravity force
h = total enthalpy
I_c = nucleation rate
J = Jacobian of transformation
n = number density of nuclei
p = static pressure
Re = Reynolds number

T = static temperature
U_i = contravariant velocities ($i = 1, 2$)
u_i = physical velocities ($i = 1, 2$)
t = physical time
x_i = Cartesian coordinates ($i = 1, 2$)
β = condensate mass fraction
$\boldsymbol{\Gamma}$ = preconditioning matrix
$\boldsymbol{\Gamma}_c$ = condensate mass generation rate
ξ_i = general curvilinear coordinates ($i = 1, 2$)
ρ = total density
ρ_s = reference density
μ = molecular viscosity
δ_{ij} = Kronecker's delta
τ_{ij} = viscous stress tensors ($i, j = 1, 2$)
κ = heat conductivity

Literature Cited

1. Weber M, Russell LM, Debenedetti PG. Mathematical modeling of nucleation and growth of particles formed by the rapid expansion of a supercritical solution under subsonic conditions. *J Supercrit Fluids*. 2002;23:65–80.
2. Helfgen B, Türk M, Schaber K. Hydrodynamic and aerosol modeling of the rapid expansion of supercritical solution (RESS-Process). *J Supercrit Fluids*. 2003;26:225–242.
3. Crist S, Sherman PM, Glass DR. Study of the highly underexpanded sonic jet. *AIAA J*. 1966;4:68–71.
4. Khalil I, Miller DR. The structure of supercritical fluid free-jet expansions. *AIChE J*. 2004;50:2697–2704.
5. Yamamoto S, Niiyama D, Shin BR. A numerical method for natural convection and heat conduction around and in a horizontal circular pipe. *Int J Heat Mass Transf*. 2004;47:5781–5792.
6. Choi YH, Merkle CL. The application of preconditioning in viscous flows. *J Comp Phys*. 1993;105:207–223.
7. Weiss JM, Smith WA. Preconditioning applied to variable and constant density flows. *AIAA J*. 1995;33:2050–2057.
8. Yamamoto S. Preconditioning method for condensate fluid and solid coupling problems in general curvilinear coordinates. *J Comp Phys*. 2005;207:240–260.
9. A program package for thermophysical properties of fluids, Ver.12.1. PROPATH group. http://www.cc.kyushu-u.ac.jp/scp/system/library/PROPATH/PROPATH.html. Accessed June, 2001.
10. Angus S, editor. *International thermodynamic table of the fluid state-3 carbon dioxide*: *Int Union Pure Appl Chem*. 1976;3.
11. Japan society of mechanical engineers. *JSME Steam Tables*. Accessed June, 1999.
12. Yamamoto S, Hagari H, Murayama M. Numerical simulation of condensation around the 3-d wing. *Trans Japan Soc Aeronaut Space Sci*. 2000;42:182–189.
13. Ishizaka K, Ikohagi T, Daiguji H. A high-resolution finite difference scheme for supersonic wet-stream flows. *Trans JSME Ser B*. 1994;60:3887–3892 (in Japanese).
14. Frenkel J. *Kinetic theory of liquids*. New York: Dover Pub, Inc., 1955.
15. Schnerr GH, Dohrmann U. Transonic flow around airfoils with relaxation and energy supply by homogeneous condensation. *AIAA J*. 1990;28:1187–1193.

Manuscript received Aug. 31, 2010, and revision received Oct. 20, 2010.